Journal of
Materials Chemistry A

Accepted Manuscript

This article can be cited before page numbers have been issued, to do this please use: C. W. Kim, W. J. Shin, M. J. Choi, J. H. Lee, S. H. Nam, Y. D. Suh, Y. S. Kang and Y. S. Kang, *J. Mater. Chem. A*, 2016, DOI: 10.1039/C6TA04526J.

ROYAL SOCIETY OF CHEMISTRY

www.rsc.org/materialsA

View Article Online
DOI: 10.1039/C6TA04526J

Journal of Materials Chemistry A

ARTICLE

Wavelength Conversion Effect-Assisted Dye-Sensitized Solar cells for Enhanced Solar Light Harvesting

Received 00th January 20xx,
Accepted 00th January 20xx

DOI: 10.1039/x0xx00000x

www.rsc.org/

Chang Woo Kim,†[a] Woo Jin Shin,†[a] Mi Jin Choi,[b] Jae Ho Lee,[a] Sang Hwan Nam,[c] Yung Doug Suh,[c] Yong Soo Kang,[b] and Young Soo Kang*[a]

In the present study, an enhanced solar light harvesting strategy based on the wavelength conversion effect is suggested in dye-sensitized solar cells (DSSCs). Incorporating β-$NaYF_4$:Yb^{3+},Er^{3+} phosphor microcrystals as a component of the DSSCs enables wavelength conversion from infrared to visible light, which maximizes the absorption of visible light by the C106 organometallic dye and produces excess current, thus enhancing the quantum efficiency. It is demonstrated that the photocurrent density generated is increased by the wavelength conversion effect of the phosphor material. The introduction of up-converting β-$NaYF_4$:Yb^{3+},Er^{3+} phosphor microcrystals dispersed in an iodide electrolyte and the use of an additional phosphor reflecting film increases the overall solar-to-electrical energy conversion efficiency (η) from 9.02% of reference DSSCs to 9.48 and 10.76%, respectively. DSSCs with phosphors contained in both the iodide electrolyte solution as well as an additional phosphor reflecting film show a highly enhanced overall efficiency of 10.90%. Herein, a strategy for effective wavelength conversion is investigated for enhanced solar light harvesting, and the results of the study contribute the most viable strategy for achieving maximum utilization of the solar spectrum.

Introduction

Since the pioneering work on electrochemical junction solar cells by the research groups of O'regan and Grätzel in 1991,[1] their strategy for the fabrication of dye-sensitized solar cells (DSSCs) by the adsorption of dye molecules on the surface of nanocrystalline TiO_2 films has been recognized as a standard technique.[2-5] Systematic components such as dye molecules, semiconductor photoanode, and electrolyte have an effect on the photovoltaic performance of DSSCs. DSSCs are now being recognized as the prospective photovoltaic energy generation devices in a field of photovoltaic solar cells due to the highly enhanced efficiency in recent report.[6-8] Depending on the components and structure of DSSCs, the photovoltaic performance is affected by light harvesting efficiency (η_{lh}), charge separation efficiency (η_{cs}), and charge collection efficiency (η_{cc}).[2-5] These factors are measured in terms of the short-circuit photocurrent density (J_{sc}), open-circuit voltage (V_{oc}), and fill factor (*FF*), and are used in determining the overall solar-to-electrical energy conversion efficiency (η). Since nearly 100% η_{cs} has already been achieved in DSSCs, η_{lh} and η_{cc} are regarded as factors that can be improved to further improve the photovoltaic performance of DSSCs.[2-5] In addition, η_{lh} is most closely related to J_{sc}, and determines the photovoltaic performance of DSSCs.

To increase η_{lh} in photovoltaics, several approaches such as combining composite materials,[9] introducing a light scattering layer,[10,11] using dual-functionalized materials,[12-15] and panchromatic absorption have been studied.[16-18] In addition, ruthenium-(II)-based organometallic molecules have been developed for use as dyes to absorb light in the wavelength range of 300-800 nm with high absorption coefficients.[19-22] These tremendous effort have been focused on enhancement of η_{lh} in the range of visible spectrum. However, these approaches are fundamentally limited in their ability to enhance the absorption of ultraviolet (UV) and Near-infrared (NIR) radiation, which constitute over 60% of the solar spectrum.[23-26] Strategies for enhancing the absorption of the UV and IR portion of the solar spectrum have received little attention for efficient DSSCs performance.

An effective alternate approach is to modify the solar wavelength spectrum available for absorption by the dye molecules, through wavelength conversion, using phosphor materials.[23,26] Introducing a phosphor material to modify the solar spectrum to be absorbed by the dye molecules is an outstanding strategy for utilizing the solar photon energy in the UV and NIR range.[27-30] The first theoretical study on utilizing a phosphor material for improving the solar cell performance was reported by Trupke et al. and the results of the study indicated that wavelength conversion of the solar spectrum would be a promising solution for improving η_{lh} of the DSSCs.[31-34] Phosphor materials can convert a portion of solar spectrum into different band of spectrum via three types of photon luminescence

[a] *Korea Center for Artificial Photosynthesis and Department of Chemistry, Sogang University, #1 Shinsu-dong, Mapo-gu, Seoul 121-742, Republic of Korea. E-mail: yskang@sogang.ac.kr.*
[b] *Center for Next Generation Dye-Sensitized Solar Cells, Department of Energy Engineering, Hanyang University, Seoul 133-791, Republic of Korea.*
[c] *Laboratory for Advanced Molecular Probing (LAMP), Research Center for Convergence Nanotechnology, Korea Research Institute of Chemical Technology, Daejeon 305-600, Republic of Korea.*
† These authors contributed equally to the research.
Electronic Supplementary Information (ESI) available: [details of any supplementary information available should be included here]. See DOI: 10.1039/x0xx00000x

View Article Online
DOI: 10.1039/C6TA04526J

conversion processes, namely up-conversion, down-conversion, and downshifting. The high-energy part of the spectrum can be converted into lower energy wavelength in the down-conversion as well as down shifting process. However, the up-conversion process converts the low-energy part of the solar spectrum into higher energy wavelength.[27-30] Combinations of up-conversion materials for photovoltaic applications have attracted attention in solar cell research, because solar light contains over 55% IR radiation. Improved DSSC performances by employing phosphor materials for wavelength conversion have been reported in recent papers.[35] Most of the reports so far have demonstrated improved DSSC performance by applying phosphors at a single position. However, the wavelength conversion effect of phosphor materials in DSSCs continues to be controversial, since there is an opinion that the wavelength conversion might be caused by the light scattering effect. Furthermore, most of the studies have been focused on enhancing solar light absorption using a combination of N719 dye and phosphor materials.[36-39]

In this work, based on our previous report on successful introduction of downshifting phosphor into DSSCs,[26] we suggest a facile strategy to improve solar light harvesting of photovoltaics by combining the wavelength conversion effect exhibited by up-conversion β-$NaYF_4$:Yb^{3+},Er^{3+} phosphor microcrystals with the C106 organometallic dye, which shows the best light-harvesting performance among new-generation high-absorption-coefficient dyes as shown in Fig. S1 (in the Supporting Information).[40,41] To the best of our knowledge, this work proposes first multi-position application of phosphors in the DSSCs, including up-conversion phosphors loaded onto TiO_2-nanoparticle films, dispersed in an iodide electrolyte and a back-reflecting phosphor film, for achieving the best light-harvesting performance. In a DSSCs containing phosphors positioned both in the iodide electrolyte solution and an additional phosphor reflecting film, J_{sc} values from 18.89 of reference DSSCs to 24.54 mA·cm^{-2} were produced. In this study, advanced DSSCs with β-$NaYF_4$:Yb^{3+},Er^{3+} phosphor microcrystals have been fabricated and the performance of DSSCs with and without phosphors have been compared. This study is expected to lead to a viable strategy for maximizing solar light harvesting.

Experimental section

Fabrication of β-$NaYF_4$:Yb^{3+},Er^{3+} Phosphor Microcrystals and Back-Reflection Films

β-$NaYF_4$:Yb^{3+},Er^{3+} phosphor microcrystals were synthesized using the hydrothermal method based on Li's work, with some modifications.[42-44] $Y(NO_3)_3$•$4H_2O$ (1.6 mmol), $Yb(NO_3)_3$•$5H_2O$ (0.36 mmol), and $Er(NO_3)_3$•$5H_2O$ (0.04 mmol) were dissolved in 40 mL of deionized water. Following this, 4 mmol of sodium citrate was added to the solution and white precipitates were observed in the solution. Upon vigorous stirring for 30 min, the solution became transparent, after which 26 mmol of NaF was added to produce white precipitates. After further stirring for 30 min, the pH was controlled to achieve acidic conditions by adding 1.0 M HNO_3 solution. The solution was transferred into a 100 mL teflon-lined stainless steel autoclave, tightly sealed, and maintained at 200 °C for 20 h in an electrical heating-oven. Subsequently, the autoclave was naturally cooled to room temperature (RT). The precipitates were separated by centrifugation, and washed with deionized water and ethanol several times. Finally, the product was dried in an oven at 80 °C for 12 h.

An up-conversion phosphor back-reflection films (UCBR) were prepared using a polyethyleneimine (PEI)-induced manual assembly method with minor modifications.[45,46] PEI solutions (1.5 mL; 4 wt%) in ethanol were spin-coated on cleaned (2 × 2) cm fluorine-doped tin oxide (FTO) glass substrates at a speed of 2000 rpm for 10 s. The β-$NaYF_4$:Yb^{3+},Er^{3+} phosphor microcrystals were then gently rubbed on the PEI-coated FTO glass substrates. The as-prepared films were then heat-treated at 450 °C for 4 h in air. Ethanol phosphor solutions (3.5 mg mL^{-1}) were dispersed by dropping 0.185 mL of the solutions on the phosphor monolayer-coated glass substrates and dried at 70 °C. A cycle of coating consisted of phosphor dispersion by dropping 0.185 mL of the prepared ethanol solution. In order to remove PEI and any organic impurities, the films were heat-treated at 450 °C for 4 h in an Ar atmosphere. By increasing the number of dispersion cycles (26 cycles), different thicknesses of β-$NaYF_4$:Yb^{3+},Er^{3+} up-converting back-reflection films were obtained.

Assembly of DSSCs with β-$NaYF_4$:Yb^{3+},Er^{3+} Phosphor Microcrystals

Assembly of DSSCs was based on Prof. Kang's report.[47] To prepare the TiO_2-film electrodes, FTO glass substrates (Pilikington, TEC 7) were sequentially cleaned with Helmanex solution, distilled water, and ethanol for 20 min in an ultrasonic bath. The photoelectrode was fabricated by spin-coating 0.1 M Ti(IV) bis(ethyl acetoacetato)-diisopropoxide solution (Aldrich) in 1-butanol (1-BuOH, 99.8%, Aldrich) onto the cleaned FTO glass substrate and heating at 450 °C for 30 min. A TiO_2-nanoparticle film layer (nTF, thickness, ~ 8 μm) was fabricated on the FTO glass by the doctor blade technique using commercial TiO_2 paste with an average 18-nm particle size (JGC C&C, PST-18NR paste). The TiO_2 scattering layer (thickness, ~ 4 μm) was sequentially loaded using commercial TiO_2 paste with an average 400-nm particle size (JGC C&C, PST-400C paste). After sintering the TiO_2-coated FTO glass substrate at 450 °C for 30 min, it was treated with a 0.5 mM titanium tetrachloride ($TiCl_4$) solution for 20 min at 70 °C, followed which an annealing process was carried out at 450 °C for 30 min. To prepare the up-conversion phosphor loaded on TiO_2 film (UCTF), an aqueous solution of the microcrystal product (2.5 mL, 0.25 wt%) was dropped 5 times directly onto the surface of the TiO_2 scattering layer (active layer was 0.16 cm^2 in area) and the TiO_2 film loaded with the microcrystals was annealed at 450 °C for 30 min. Each working electrode was dipped into 0.5 mM of the C106 dye (Dyesol) dissolved in acetonitrile (99.9%, Wako) and tert-butanol (99%, Wako) (v/v, 1:1) for 18 h at RT. The electrodes were washed with acetonitrile to remove residues and were then dried.

Electrolytes composed of 0.6 M 1-methyl-3-propylimidazolium iodide (MPII, ≥ 98%, Aldrich), 0.03 M iodine (I_2, ≥ 99.8%, Aldrich), 0.5 M tert-butylpyridine (t-BP, 96%, Aldrich), 0.1 M lithium iodide (LiI, 99.9%, Aldrich), and 0.1 M guanidine thiocyanate (GuSCN, ≥ 97%, Aldrich) were dissolved in acetonitrile/valeronitrile (VN, 99.5%, Aldrich) (v/v, 85:15). To prepare the up-conversion phosphors dispersed in iodide electrolyte solution (UCEL), 0.06 g of the β-$NaYF_4$:Yb^{3+},Er^{3+} phosphor microcrystals was dispersed

View Article Online
DOI: 10.1039/C6TA04526J

homogenously at 50 °C for 1 h into 2 mL of the aforementioned electrolyte solution to obtain a 4 wt% solution. The platinum counter electrode was spin-coated with 0.1 M chloroplatinic acid (H_2PtCl_6, 8 wt% in H_2O, Aldrich), which was dissolved in 2-propanol (Aldrich), and was calcinated at 450 °C for 30 min. The working and counter electrodes were both assembled using 60 µm of hot-melted Surlyn (Solaronix).

Results and discussion

β-$NaYF_4$:Yb^{3+},Er^{3+} micro-rod crystals were hydrothermally synthesized using sodium citrate as a chelating agent.[42-44] Typical scanning electron microscopy (SEM) images, energy-dispersive X-ray spectroscopy (EDS) maps, high-resolution transmission electron microscopy (HRTEM) images, and selected-area electron diffraction (SAED) patterns of the crystal structure of β-$NaYF_4$:Yb^{3+},Er^{3+} phosphor crystals along with the lattice distance calculations are shown in **Fig. 1** and Fig. S2. The HRTEM and SAED patterns viewed along the [100] direction show that the β-$NaYF_4$:Yb^{3+},Er^{3+} phosphor microcrystals grew along the [001] direction as the c-axis. A well-defined microcrystal in a representative micro-rod exhibited a length of ~ 7.8 µm and a diameter of ~ 0.86 µm. The corresponding elemental mapping images indicate that Yb^{3+} and Er^{3+} ions were spatially dispersed in the $NaYF_4$ host crystal structure. Based on the relationship between the initial pH and the charge on citrate, it was determined that the β-$NaYF_4$:Yb^{3+},Er^{3+} phosphor micro-rod crystals grew at pH 3.13, where crystal growth along the [001] direction is much faster than that in the other directions, which resulted in the formation of [001]-oriented micro-rod crystals.[48] This result is also consistent with the dominant peak intensity of the (100) axis observed in the XRD patterns shown in Fig. 2 and Fig. S3. In addition to the [001] growth direction, the β-$NaYF_4$:Yb^{3+},Er^{3+} phosphor microcrystals also grew to some extent along six energetically equivalent {$10\bar{1}0$} side facets [($10\bar{1}0$), ($\bar{1}010$), ($0\bar{1}10$), ($01\bar{1}0$), ($\bar{1}100$), and ($1\,\bar{1}\,00$)], as shown in the XRD patterns of pristine β-$NaYF_4$:Yb^{3+},Er^{3+} phosphor micro-rod crystals.

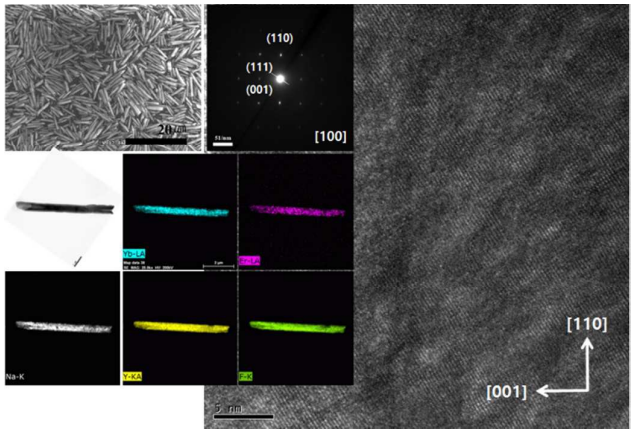

Fig. 1 Microscopic observations of the β-$NaYF_4$:Yb^{3+}, Er^{3+} phosphor microcrystals. The HRTEM image corresponds to the SAED pattern. EDS elemental mappings of the same crystal region indicate the spatial distribution of Na, Y, F, Yb, and Er.

To achieve up-conversion emission, the β-$NaYF_4$ host lattice crystals were doped with a sensitizer (Yb^{3+}) and an activator (Er^{3+}). Since Yb^{3+} and Er^{3+} ions were intercalated into the β-$NaYF_4$ host lattice crystals, the peak positions of the β-$NaYF_4$:Yb^{3+}, Er^{3+} phosphor microcrystals shifted to lower 2θ angles (PDF#281192, space group: $P6_3/m$), compared to the values provided in the standard JCPDS card of pristine β-$NaYF_4$ microcrystals without Yb^{3+} and Er^{3+} (PDF#160334, space group: $P6_3/m$).[49] The peak of (100) shows negligible lattice difference in pure and doped β-$NaYF_4$ such as 0.002 nm.

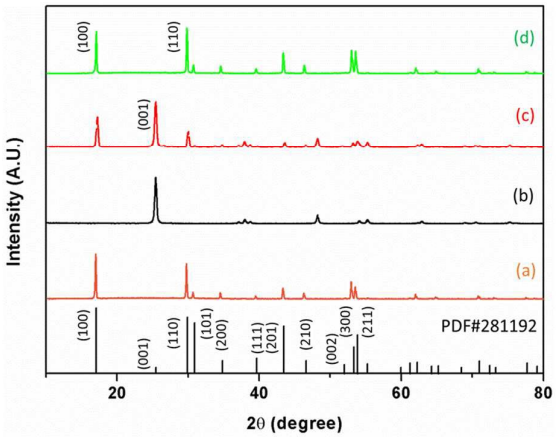

Fig. 2 XRD results of (a) pristine β-$NaYF_4$:Yb^{3+}, Er^{3+} phosphor microcrystals, (b) TiO_2 nanoparticle electrode used as a reference for comparison, (c) phosphors on a TiO_2-film electrode (UCTF), and (d) back-reflecting film (UCBR). Anatase TiO_2 (PDF#841285) and β-$NaYF_4$:Yb^{3+}, Er^{3+} (PDF#281192) were used.

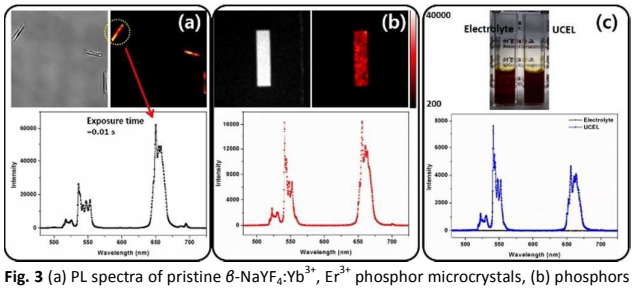

Fig. 3 (a) PL spectra of pristine β-$NaYF_4$:Yb^{3+}, Er^{3+} phosphor microcrystals, (b) phosphors on TiO_2 nanoparticle films (UCTF), and (c) phosphor microcrystals dispersed in the electrolyte (UCEL).

The as-synthesized β-$NaYF_4$:Yb^{3+},Er^{3+} phosphor microcrystals were introduced onto the spherical TiO_2 particle layer as a photoanode (UCTF), by dispersing the microcrystals in the electrolyte solution (UCEL). In addition, the microcrystals were casted as a back-reflecting film (UCBR) in the DSSCs. Fig. 2 shows the XRD patterns of the TiO_2-nanoparticle-film electrode (nTF, which was used as a reference electrode), up-conversion phosphor on the TiO_2-nanoparticle-film (UCTF) photoanode and up-conversion phosphor film for the back-reflecting (UCBR) plate. The XRD patterns indicate that the β-$NaYF_4$:Yb^{3+},Er^{3+} phosphor microcrystals were successfully loaded on the nTF. The {$10\bar{1}0$}-orientated β-$NaYF_4$:Yb^{3+},Er^{3+} film on the transparent glass was employed as the back-reflection film via the PEI-induced manual assembly technique.[45,46] The as-synthesized β-$NaYF_4$:Yb^{3+},Er^{3+} phosphor microcrystals were assembled as UCBR with ~ 30 µm film thickness, as shown in Fig. S4.

View Article Online
DOI: 10.1039/C6TA04526J

The photoluminescence (PL) spectra of the pristine β-$NaYF_4$:Yb^{3+},Er^{3+} phosphor microcrystals, UCTF, and the up-conversion phosphor dispersed in the iodide electrolyte solution (UCEL) were compared and results are shown in Fig. 3. Upon excitation in the wavelength range of 900-1050 nm (Fig. S5), the PL spectra of pristine β-$NaYF_4$:Yb^{3+},Er^{3+} phosphor microcrystals, UCTF, and UCEL showed two strong luminescence bands at 510-560 nm and 640-675 nm, as shown in Fig. 3(a), (b), and (c), respectively. The top images in Fig. 3(a) are the optical microscopic images of pristine β-$NaYF_4$:Yb^{3+},Er^{3+} phosphor microcrystals acquired with an exposure time 0.01 s. Similarly, bright field optical microscopic images (top) and PL spectrum (bottom) of phosphor deposited on TiO_2-nanoparticle films are shown in Fig. 3(b).

In the top image of Fig. 3(c), the emission color of UCEL is compared with that of the pristine electrolyte. As is evident from the Fig. 3, no emission was observed from the electrolyte. Since the PL spectra were results of the energy transfer from Yb^{3+} (sensitizer) to Er^{3+} (activator) in the $NaYF_4$ host material lattice, the light emitted at both 510-560 nm and 640-675 nm were in the absorption range of the C106 organometallic dye.[40,41] From absorption and emission spectra of β-$NaYF_4$:Yb^{3+},Er^{3+} phosphor microcrystals, quantum efficiency (QE) was calculated 2.98% with following equation (1) in Fig. 4.[50,51]

$$\%QE = \frac{\#\ of\ emitted\ photons}{\#\ of\ exited\ photons}\ X\ 100 \quad (1)$$

In here, number of excited photons was calculated from [(PL area under the curve of excitation spectra)$_{Reference}$ X (1/%Reflectance)$_{Reference}$ X (% Reflectance)$_{sample}$] and number of emitted photons was calculated with (PL area under the curve of emission spectra)$_{sample}$. Reference is alumunimun foil and sample is up-conversion phosphor.

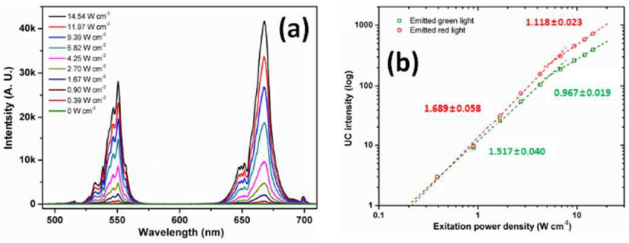

Fig. 4 PL spectra dependence on power density of the β-$NaYF_4$:Yb^{3+},Er^{3+} phosphor microcrystals. (a) PL spectra and (b) log (UC intensity) vs log (power density) graph.

As shown in Fig. 4, the efficiency of up-conversion process was determined as a dependence on power density. The emission intensity curve increases as power density increases to around 10 W· cm^{-2}. Considering this result, it would be expected that this phosphor microcrystal produces constant QE under indoor application of DSSCs. From the XRD patterns, microscopic images, and PL spectra, it may be concluded that the β-$NaYF_4$:Yb^{3+},Er^{3+} phosphor microcrystals were well-incorporated into the DSSC components as UCTF and UCEL. The significantly increased intensity of the 510-560 nm and 640-675 nm luminescence bands in the cases of UCTF and UCEL, respectively, is expected to be a key factor in enhancing solar light harvesting via the wavelength conversion effect. Our hypothesis on UCTF, UCEL, UCBR, and UCEB (simultaneously applied UCEL and UCBR) was verified for the photovoltaic performance measurements, which are shown in Scheme 1.

To determine the η_{lh} as a result of wavelength conversion, β-$NaYF_4$:Yb^{3+},Er^{3+} phosphor microcrystals were introduced into the DSSCs and the optimal positions of the β-$NaYF_4$:Yb^{3+},Er^{3+} phosphor microcrystals in the DSSCs are illustrated in Schemes 1. β-$NaYF_4$:Yb^{3+},Er^{3+} phosphor microcrystals were loaded on the TiO_2-nanoparticle-film (UCTF, Scheme 1(a)) and dispersed in the iodide electrolyte (UCEL, Scheme 1(b)). A {$10\bar{1}0$}-orientated β-$NaYF_4$:Yb^{3+}, Er^{3+} phosphor film was employed as a UCBR, which was an external component, as shown in Scheme 1(c). For achieving an integrated wavelength conversion effect, β-$NaYF_4$:Yb^{3+}, Er^{3+} phosphor microcrystals were simultaneously dispersed in the iodide electrolyte and used as UCEB, as shown in Scheme 1(d).

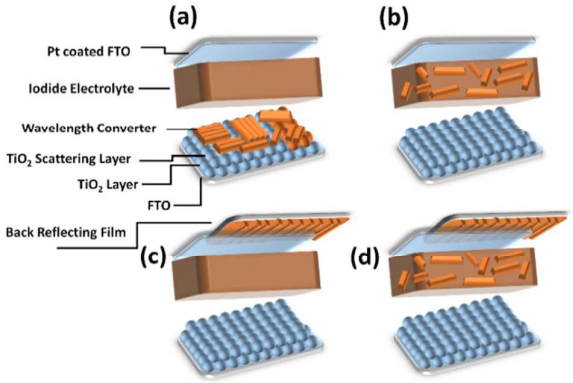

Scheme 1. Schematic of the locations of the wavelength conversion phosphor microcrystals on TiO_2 film (a, UCTF), phosphor dispersed in the electrolyte (b, UCEL), back-reflecting film (c, UCBR), and phosphors both dispersed in the electrolyte as well as introduced in the back-reflecting film (d, UCEB).

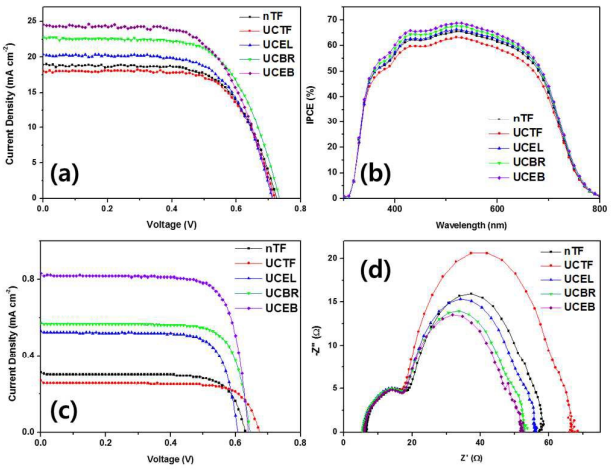

Fig. 5 Photovoltaic characteristics and electrochemical impedance measurements as a function of the location of the β-$NaYF_4$:Yb^{3+}, Er^{3+} phosphor microcrystals. (a) I-V curves under 1-sun, (b) IPCE, (c) I-V curves under IR range (> 815 nm) and (d) Nyquist plots under 1-sun.

Fig. 5 shows the photovoltaic characteristics of nTF, UCTF, UCEL, UCBR, and UCEB measured under 1-sun and IR range condition. The J_{sc} of UCEL was 20.38 mA·cm^{-2}, which was distinguishable from the

View Article Online
DOI: 10.1039/C6TA04526J

value of 18.89 mA·cm^{-2} obtained for nTF. The V_{oc} values of UCEL and nTF were 0.712 V and 0.726 V, respectively. Interestingly, when the β-$NaYF_4$:Yb^{3+},Er^{3+} film was utilized as UCBR, J_{sc} increased to 22.73 mA·cm^{-2}, which was higher than the corresponding value for nTF. Since the J_{sc} of the UCBR film increased and the initial value of V_{oc} was retained, this external reflection film is a promising option for enhancing light-harvesting in DSSCs. This finding indicates that the increase in the J_{sc} value originated predominantly from the reflected illumination and not from wavelength conversion, when β-$NaYF_4$:Yb^{3+},Er^{3+} phosphor was used as an external film on the back side. Unexpectedly, when the β-$NaYF_4$:Yb^{3+},Er^{3+} phosphor microcrystals were simultaneously applied as UCEL and UCBR in the DSSCs (UCEB), the photocurrent densities of the DSSCs drastically increased, even as the initial V_{oc} value was retained. As shown in Fig. 5 (a), the J_{sc} value of UCEB increased from 18.89 to 24.54 mA·cm^{-2} for nTF, while V_{oc} remained at 0.714 V. There was no significant change in *FF*. It is interesting to note that the remarkable difference between nTF as a reference DSSCs and UCEB was caused by the drastic increase in J_{sc}, and resulted in enhanced solar light harvesting. The J_{sc} value of DSSCs containing β-$NaYF_4$:Yb^{3+},Er^{3+} phosphors also increased drastically. However, their V_{oc} value did not decrease. The *FF* values of UCEL, UCBR, and UCEB remained constant. The β-$NaYF_4$:Yb^{3+},Er^{3+} phosphor microcrystals are quite suitable for use as components of DSSCs, to achieve high photovoltaic performance. However, when the β-$NaYF_4$:Yb^{3+},Er^{3+} phosphor microcrystals were loaded onto the nTF, the photocurrent densities of the DSSCs did not increase significantly, and the presence of the microcrystals caused the photovoltaic performance of the DSSCs to be deteriorated. This could be a result of the larger amount of dye molecules adsorbed on nTF compared to the amount on UCTF.[52] The amount of adsorbed dye molecules would be lower in UCTF as a result of the decreased contact area between the loaded phosphor microcrystals and nTF.[52] Considering that the amount of adsorbed dye molecules is directly related to η_{lh}, the amount of adsorbed dye molecules plays a key role in improving the photovoltaic performance of UCTF, as well as the up-conversion effect of the β-$NaYF_4$:Yb^{3+},Er^{3+} phosphor microcrystals. This result agrees with the results obtained by comparing the incident photon-to-current efficiency (IPCE) values between nTF and UCTF. A distinguishable difference in the IPCE was observed between β-$NaYF_4$:Yb^{3+},Er^{3+} phosphor-loaded DSSCs and reference DSSCs containing nTF, as shown in Fig. 5 (b). The higher IPCE value of nTF compared to that of UCTF was related to the η_{lh} of the dye molecules. On the other hand, the IPCE values of UCEL and UCBR were higher than that of nTF in the wavelength range of 370-790 nm. Among the various configurations, UCEB exhibited the highest IPCE value (68.8%) at 520 nm. nTF, UCEL, and UCBR exhibited IPCE values of 65.6%, 66.4%, and 67.7%, respectively. However, photocurrent density of each DSSCs is not following same order like IPCE because of the high photon flux and limited absorption spectrum by cut-off filter.[53] Hence, it is reasonably accepted that photocurrent density are enhanced through wavelength conversion effect from phosphor in DSSCs. Especially, I-V curves of each DSSCs containing nTF, UCTF, UCEL, UCBR and UCEB were measured and compared under NIR range using cut-off filter over 815 nm in Fig. 5 (c). As the result of I-V curves and IPCE values under 1-sun illumination, the J_{sc} value of UCEB reached to 0.83 from 0.31 mA·cm^{-2} for nTF under NIR range. UCTF, UCEL and UCBR produced 0.27, 0.53 and 0.58 mA·cm^{-2}, respectively. It indicates that DSSCs containing phosphor are well-photoactivated under NIR range and result in the increased photovoltaic performance. A higher IPCE would be expected when phosphors are applied in multiple positions of the DSSCs like in the case of UCEB, compared to its introduction at a single position like in the cases of UCEL and UCBR.[23-26] This indicates that the use of the UCEB configuration is more favorable for harvesting solar light, compared to the use of the UCEL and UCBR configurations. Impedance values were measured and compared among nTF, UCTF, UCEL, UCBR, and UCEB and the results are shown in Fig. 5 (d). In the Nyquist plots of the samples, the presence of a semicircle at high frequency, which is related to the impedance at the interface between the redox electrolyte and the platinum counter electrode, indicates low charge-transfer resistance.[23-26] Since the second semicircle is derived from the recombination resistance at the interface between the C106 dye/TiO_2 layer and electrolyte, the J_{sc} value increases in the following order: UCEB > UCBR > UCEL > UCTF under 1-sun illumination. This ordering was also observed in the impedance result under NIR range as shown in Fig. S6. Although the phosphor microcrystals are present in the electrolyte in the cases of UCEL and UCEB, they do not affect the charge transfer resistance because the phosphor microcrystals in the electrolyte solution are not chemically bonded with the iodide electrolyte. In this aspect, it indicates that higher charge transfer rate overcome recombination rate at interface because of enhanced photocurrent from UCEB compared with others.

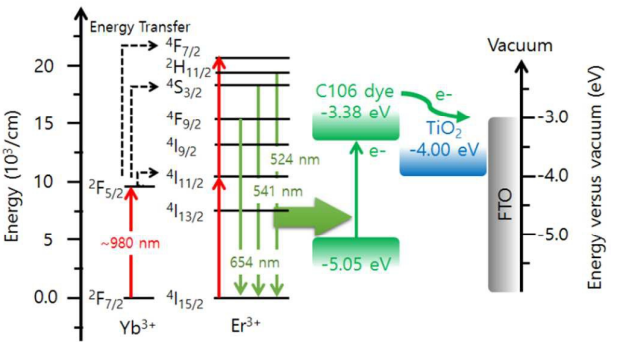

Scheme 2. Schematic illustration of the proposed energy transfer mechanism in the TiO_2 electrode containing β-$NaYF_4$:Yb^{3+}, Er^{3+} phosphor microcrystals and C106 organic dye.

Among them, UCEB exhibits the highest η_{lh} and photovoltaic performance, owing to its low interfacial impedance for charge transfer. In order to assess the up-conversion effects of the β-$NaYF_4$ phosphor microcrystals with and without Yb^{3+} and Er^{3+}, the J_{SC} values of nTF, UCTF, UCEL, UCBR, and UCEB with and without Yb^{3+} and Er^{3+} were compared and the results are shown in Fig. S7. The J_{sc} values of UCTF, UCEL, UCBR, and UCEB containing Yb^{3+} and Er^{3+} as dopants were higher than those of the β-$NaYF_4$ microcrystals without Yb^{3+} and Er^{3+} (nUCTF, nUCEL, nUCBR, and nUCEB). In particular, it is interesting to note the remarkable difference in J_{sc} between UCEB (24.54 mA·cm^{-2}) and nUCEB (22.85 mA·cm^{-2}). Since Yb^{3+} and Er^{3+} played the roles of sensitizer and activator in the

View Article Online
DOI: 10.1039/C6TA04526J

phosphor microcrystals for harvesting visible light from the NIR wavelength regime by the up-conversion effect, the increase in the J_{sc} values of UCTF, UCEL, UCBR, and UCEB is remarkable.

According to the PL spectra shown in Fig. 3, the *β*-$NaYF_4$:Yb^{3+},Er^{3+} phosphor microcrystals absorbed NIR radiation at 980 nm and emitted two strong luminescence bands at 510-560 and 640-675 nm. The peak at 524 nm is assigned to the transition from $^2H_{11/2}$ to $^4I_{15/2}$, whereas the peak at 541 nm is assigned to the transition from $^4S_{3/2}$ to $^4I_{15/2}$. Further, the peak at 654 nm is assigned to the transition from $^4F_{9/2}$ to $^4I_{15/2}$. These PL peaks are located in the absorption wavelength range of the C106 dye, as shown in Scheme 2. The emission wavelength of the up-conversion portions of solar light is required to be absorbed by the C106 dye in order to achieve improvement in the photovoltaic performance. The C106 molecule exhibits λ_{max} absorption at ~550 nm. Therefore, the *β*-$NaYF_4$:Yb^{3+},Er^{3+} phosphor microcrystals were able to provide a large portion of emitted light at around 550 nm (541, 510-560 nm) by up-conversion of the NIR radiation to support maximum absorption by the C106 dye. The up-conversion of solar light by the prepared *β*-$NaYF_4$:Yb^{3+},Er^{3+} phosphor microcrystals are shown in Scheme 2.

Table 1 Photovoltaic performance as a function of the positions of the β-$NaYF_4$:Yb^{3+}, Er^{3+} phosphor microcrystals in the DSSCs.

DSSC[a)]	J_{sc} (mA cm^{-2})	V_{oc} (V)	*FF* (%)	*η* (%)	$\Delta\eta$[b)] (%)
nTF	18.89±0.47	0.726±0.021	65.76	9.02	
UCTF	18.00±0.55	0.719±0.018	68.35	8.86	
UCEL	20.38±0.52	0.712±0.014	65.39	9.48	5.09
UCBR	22.73±0.50	0.734±0.005	64.45	10.76	19.29
UCEB	24.54±0.44	0.714±0.019	62.19	10.90	20.84

a)denoted in Scheme 1; b)$^{\Delta}\eta = (\eta - \eta_{nTF})/\eta_{nTF}$ X 100%

Based on careful characterization of the PL spectra and assessment of the photovoltaic performance in DSSCs, it was concluded that the internal incorporation of *β*-$NaYF_4$:Yb^{3+},Er^{3+} phosphor microcrystals into DSSCs with external loading phosphor films as a reflecting plate was a promising strategy for improving the photovoltaic performance of the DSSCs, as shown in Table 1 and Fig. S8. Our findings also support the conclusion that maximum DSSC performance would be obtained from both the external back-reflecting film by scattering and wavelength conversion effect and the internal introduction of phosphors into the electrolyte solution of DSSCs. In the present study, the up-converting *β*-$NaYF_4$:Yb^{3+},Er^{3+} phosphor microcrystals were incorporated into the DSSC components both internally and externally to promote solar light harvesting. Considering the proportion of UV and IR radiation in the total solar light, the use of down-conversion and up-conversion processes appears to be a promising approach for increasing the light harvesting efficiency. The effect of applying downshifting *t*-$LaVO_4$:Dy^{3+} phosphors[26] internally and externally to DSSCs for wavelength conversion from visible to UV regimes, simultaneously with up-conversion phosphors, will be reported in the next study.

Conclusions

In conclusion, the results of the study suggest that the most viable strategy for maximizing solar light harvesting is by incorporating up-conversion phosphors in the DSSC components. In the present study, the incorporation of up-conversion phosphors provided a straightforward method for enhancing the photovoltaic performance of DSSCs via wavelength conversion. Additionally, solar light harvesting was improved with the use of a back-reflecting film containing phosphors. This work on the use of phosphors indicates that *β*-$NaYF_4$:Yb^{3+} and Er^{3+} up-converting phosphor microcrystals can be potentially used in the internal and external components of DSSCs. When the phosphor microcrystals were integrated into DSSCs containing the C106 organometallic dye (which has a high IPCE, owing to its large optical absorption coefficient), the photovoltaic performance was enhanced via the wavelength conversion effect. Based on this study, we expect that this methodology can be applied to other wavelength converters, such as UV/NIR/IR-responsive phosphors, to improve light harvesting in DSSCs.

Acknowledgements

This research was supported by the Korea Center for Artificial Photosynthesis (KCAP) located in Sogang University, funded by the Ministry of Science, ICT, and Future Planning (MSIP) through the National Research Foundation of Korea (No. 2009-0093885) and the Brain Korea 21 Plus Project funded by the Ministry of Education, Science, and Technology (MEST) of Korea. The DRC Program (Y.D.S., 2014) funded from the National Research Council of Science and Technology, and by the grant (Y.D.S., KK1603-A00) from Korea Research Institute of Chemical Technology.

Notes and references

1 B. Oregan, M. Grätzel, *Nature*, 1991, **353**, 737-740.
2 N.-G. Park, J. *Electrochem. Sci. Technol.*, 2010, **1**, 69-74.
3 K. Zhu, S-R. Jang, A. J. Frank, *J. Phys. Chem. Lett.*, 2011, **2**, 1070-1076.
4 Y. Ren, Y. Li, S. Chen, J. Liu, J. Zhang, P. Wang, *Energy Environ. Sci.*, 2016, **9**, 1390-1399.
5 B. E. Hardin, E. T. Hoke, P. B. Armstrong, J-H. Yum, P. Comte, T. Torres, J. M. J. Fréchet, M. K. Nazeeruddin, M. Grätzel, M. D. McGehee, *Nature Photon*., 2009, **3**, 406-411.
6 S. Zhang, X. Yang, Y. Numata, L. Han, *Energy Environ. Sci*., 2013, **6**, 1443-1464.
7 J. H. Im, C. R. Lee, J. W. Lee, S. W. Park, N. G. Park, *Nanoscale,* 2011, **3**, 4088-4093.
8 N. J. Jeon, J. H. Noh, Y. C. Kim, W. S. Yang, S. Ryu, S. I. Seok, *Nature Mat*., 2014, **13**, 897-903.
9 H. Yu, J. Roh, J. Yun, J. Jang, *J. Mater. Chem. A,* 2016, **4**, 7322-7329.
10 L. Liang, Y. Liu, X-Z. Zhao, *Chem. Commun*. 2013, **49**, 3958-3960.
11 K. Mahmood, H. J. Sung, *J. Mater. Chem. A*, 2014, **2**, 5408-5417.
12 W. Liao, D. Zheng, J. Tian, Zhiqun Lin, *J. Mater. Chem. A*, 2015, **3**, 23360-23367.
13 J. Wu, J. Wang, J. Lin, Y. Xiao, G. Yue, M. Huang, Z. Lan, Y. Huang, L. Fan, S. Yin, T. Sato, *Sci. Rep*., 2013, **3**, 2058-2063.

View Article Online
DOI: 10.1039/C6TA04526J

14 J. Roh, S. H. Hwang, J. Jang, *ACS Appl. Mater. Inter.*, 2014, **6**, 19825-19832.
15 L. Liang, Y. Liu, C. Bu, K. Guo, W. Sun, N. Huang, T. Peng, B. Sebo, M. Pan, W. Liu, S. Guo, X-Z. Zhao, *Adv. Mater*., 2013, **25**, 2174-2180.
16 K. Lee, S. W. Park, M. J. Ko, K. Kim, N.-G. Park, *Nature Mat*., 2009, **8**, 665-671.
17 J. H. Noh, S. H. Im, J. H. Heo, T. N. Mandal, S. I. Seok, *Nano Lett*., 2013, **13**, 1764-1769.
18 J.-H Yum, E. Baranoff, S. Wenger, M. K. Nazeeruddin, M. Grätzel, *Energy Environ. Sci*. 2011, **4**, 842-857.
19 C-H. Shan, X-J. Sang, H. Zang, J-S. Li, W-L. Chen, Z-M. Su, E-B. Wang, *Inorg. Chem. Commun*., 2014, **50**. 13-16.
20 K. Kakiage, Y. Aoyama, T. Yano, K. Oya, T. Kyomen, M. Hanaya, *Chem. Commun.*, 2015, **51**, 6315-6317.
21 A. Reynal, A. Forneli, E. Palomares, *Energy Environ. Sci*., 2010, **3**, 805-812.
22 C-Y. Chen, N. Pootrakulchote, M-Y. Chen, T. Moehl, H-H. Tsai, S. M. Zakeeruddin, C-G. Wu, M. Grätzel, *Adv. Energy Mater.*, 2012, **2**, 1503-1509.
23 T. F. Schulze, T. W. Schmidt, *Energy Environ. Sci.*, 2015, **8**, 103-125.
24 X. Dang, J. Qi, M. T. Klug, P-Y. Chen, D. S. Yun, N. X. Fang, P. T. Hammond, A. M. Belcher, *Nano Lett*., 2013, **13**, 637-642.
25 I-K. Ding, J. Zhu, W. Cai, S-J. Moon, N. Cai, P. Wang, S. M. Zakeeruddin, M. Grätzel, M. L. Brongersma, Y. Cui, M. D. McGehee, *Adv. Energy Mater.*, 2011, **1**, 52-57.
26 C. W. Kim, D. K. Kim, W. J. Shin, M. J. Choi, Y. S. Kang, Y. S. Kang, *Nano Energy*, 2015, **13**, 573-581.
27 H.-Q. Wang, M. Batentschuk, A. Osvet, L. Pinna, C. J. Brabec, *Adv. Mater.*, 2011, **23**, 2675-2680.
28 N. Chander, A. F. Khan, V. K. Komarala, S. Chanwla, V. Dutta, *Prog. Photovolt: Res. Appl.*, 2016, **24**, 692-703.
29 P. Zhao, Y. Zhu, X. Yang, X. Jiang, J. Shen, C. Li, *J. Mater. Chem. A*, 2014, **2**, 16523-16530.
30 J. Shen, Z. Li, R. Cheng, Q. Luo, Y. Luo, Y. Chen, X. Chen, Z. Sun, S. Huang, *ACS Appl. Mater. Inter*., 2014, **6**, 17454-17462.
31 W. Zou, C. Visser, J. A. Maduro, M. S. Pshenichnikov, J. C. Hummelen, *Nature Photon.*, 2012, **6**, 560-564.
32 X. Huang, S. Han, W. Huang, X. Liu, *Chem. Soc. Rev.*, 2013, **42**, 173-201.
33 Z. R. Abrams, A. Niv, X. Zhang, *J. Appl. Phys*., 2011, **109**, 114905.
34 Z. Hameiri, A. M. Soufiani, M. K. Juhl, L. Jiang, F. Huang, Y.-B. Cheng, H. Kampwerth, J. W. Weber, M. A. Green, T. Trupke, *Prog. Photovolt: Res. Appl.*, 2015, **23**, 1697-1705.
35 P. Ramasamy, J. Kim, *Chem. Commun*., 2014, **50**, 879-881.
36 L. Liang, Y. Liu, X-Z. Zhao, *Chem. Commun.*, 2013, **49**, 3958-3960.
37 Y. Li, G. Wang, K. Pan, B. Jiang, C. Tian, W. Zhou, H. Fu, *J. Mater. Chem*., 2012, **22**, 20381-20386.
38 Z. Hosseini, W-K. Huang, C.-M. Tsai, T-M. Chen, N. Taghavinia, E. W-G. Diau, *ACS Appl. Mater. Inter.*, 2013, **5**, 5397-5402.
39 P-K. Chuang, Y-J. Lin, C-M. Chen, C-C. Chang, *J. Electrochem. Soc.*, 2014, **161**, H404-H409.
40 W. H. Howie, F. Claeyssens, H. Miura, L. M. Peter, *J. Am. Chem. Soc*., 2008, **130**, 1367-1375.
41 L. H. Nguyen, H. K. Mulmudi, D. Sabba, S. A. Kulkarni, S. K. Batabyal, K. Nonomura, M. Grätzel, S. G. Mhaisalkar, *Phys. Chem. Chem. Phys.*, 2012, **14**, 16182-16186.
42 C. Li, J. Yang, P. Yang, X. Zhang, H. Lian, J. Lin, *Cryst. Growth Des*., 2008, **8**, 923-929.
43 C. Li, Z. Quan, J. Yang, P. Yang, J. Lin, *Inorg. Chem*., 2007, **46**, 6329-6337.
44 C. Li, J. Yang, Z. Quan, P. Yang, D. Kong, J. Lin, *Chem. Mater*., 2007, **19**, 4933-4942.
45 C. W. Kim, Y. S. Son, A. U. Pawar, M. J. Kang, J. Y. Zheng, V. Sharma, P. Mohanty, Y. S. Kang, *J. Mater. Chem. A*, 2014, **2**, 19867-19872.
46 C. W. Kim, S. J. Yeob, H-M. Cheng, Y. S. Kang, *Energy Environ. Sci.*, 2015, **8**, 3646-3653.
47 W. Cho, Y. R. Kim, D. Song, H. W. Choi, Y. S. Kang, *J. Mater. Chem. A,* 2014, **2**, 17746-17750.
48 A. U. Pawar, C. W. Kim, M. J. Kang, Y. S. Kang, *Nano Energy*, 2016, **20**, 156-167.
49 Q. Wang, Y. Liu, B. Liu, Z. Chai, G. Xu, S. Yu, J. Zhang, *Cryst. Eng. Comm*., 2013, **15**, 8262-8272.
50 A. P. Jadhav, A. U. Pawar, U. Pal, Y. S. Kang, *J. Mater. Chem. C.,* 2014, **2**, 496-500.
51 J-C. Boyer, F. C. J. M. V. Veggel, *Nanoscale*, 2010, **2**, 1417-1419.
52 B. Ding, B. J. Lee, M. J. Yang, H. S. Jung, J.-K. Lee, *Adv. Energy Mater.* 2011, **1**, 415-421.
53 J.-W. Jang, S. H. Cho, G. Magesh, Y. J. Jang, J. Y. Kim, W. Y. Kim, J. K. Seo, S. J. Kim, K.-H. Lee, J. S. Lee, *Angew. Chem. Inter. Ed.* 2014, **53**, 5852-5857.